INSTITUTE OF PHYSICS PUBLISHING JOURNAL OF OPTICS A: PURE AND APPLIED OPTICS

J. Opt. A: Pure Appl. Opt. **4** (2002) S135–S139 PII: S1464-4258(02)28864-9

Three- and four-wave model of modulation instability fibre laser

P Honzatko, P Peterka and J Kanka

Institute of Radio Engineering and Electronics, Academy of Sciences of the Czech Republic, Chaberská 57, 182 51 Praha 8, Czech Republic

E-mail: honzatko@ure.cas.cz

Received 17 September 2001, in final form 9 April 2002
Published 14 August 2002
Online at stacks.iop.org/JOptA/4/S135

Abstract
A truncated three- and four-wave model of a fibre ring laser based on modulation instability is developed. Stationary regimes of the laser are studied through a linear stability analysis. The threshold power for the onset of the modulation instability regime for the three-wave model is derived and it is shown that no threshold exists in the four-wave model. The basic features of models are compared with experimental results obtained for a modulation instability fibre σ-laser.

Keywords: Modulation instability, fibre laser

1. Introduction

Modulation instability (MI) refers to spontaneous growth of sidebands at the expense of the continuous wave due to four-wave mixing in a nonlinear dispersive medium [1, 2]. In the anomalous group-velocity dispersion regime of an optical fibre the phase mismatch between the pump and sidebands due to dispersion is compensated by the action of self-phase and cross-phase modulations [3]. The use of the initial amplitude modulation for inducing the MI was suggested by Hasegawa in 1984 [4] and observed in 1986 [5].

MI can be utilized in an optical pulse source with a high repetition rate. Recently, Franco *et al* reported pulse trains with repetition rates up to 130 GHz in an MI fibre ring laser (FRL) [6]. Stable continuous operation with a well-defined repetition rate was achieved in a fibre ring laser with a Fabry–Perot etalon [7] and fibre σ-laser [8]. The main advantage of the MI fibre laser is its simplicity. A high-repetition-rate pulse train can be produced without expensive modulators and electronic equipment. Moreover, repetition rates not achievable by active mode-locking can be obtained.

In this paper we investigate the dynamics of an MI FRL. The configuration of the laser is identical to the MI FRL investigated by Nakazawa *et al* [7]. The MI FRL is composed of a section of a nonlinear optical fibre, lumped amplifier, Butterworth bandpass filter, Fabry–Perot etalon and output coupler, as can be seen in figure 1. If changes of the pulses per round trip are small, the evolution of the signal wave in the MI FRL is governed by a complex Ginzburg–Landau equation (CGLE), also known as a Haus master equation [9]:

$$\mathrm{i}\partial_z u - \frac{\beta_2}{2}\partial_{tt}u + R|u|^2u = \mathrm{i}b\partial_{tt}u + \mathrm{i}g(Q_1)u - \mathrm{i}lu \qquad (1)$$

where β_2 is the dispersion, R is the nonlinear coefficient, b is the filtering coefficient, l is the loss, $g(Q_1) = g_0/(1 + Q_1/P_s)$ describes the action of saturable gain with $Q_1 = 1/T\int|u|^2\mathrm{d}t$ corresponding to the average power, g_0 is the unsatured gain and P_s is the saturation power. Exact periodic solutions of the CGLE are known for some special cases [10] and are not available for the general equation (1). Therefore we have developed two simple approximate models of the MI FRL. The three-wave model corresponds to the MI FRL operation with an odd spectrum (meaning odd number of lines in a symmetrical spectrum) and the four-wave model simulates the operation of the induced MI FRL with an even spectrum. The results obtained by using the models are compared to the experimental ones obtained with the MI fibre σ-laser. A similar truncated three-wave model was used for the investigation of MI dynamics in an optical fibre [11, 12] and synchronously pumped passive resonator [13, 14].

2. Three-wave model of the fibre ring laser

Let us suppose that the MI FRL laser initially works in a stationary CW regime. This means that it generates one strong line at the frequency ω_0. Let us allow for the evolution of two sidebands with the detuning Ω defined by the free spectral

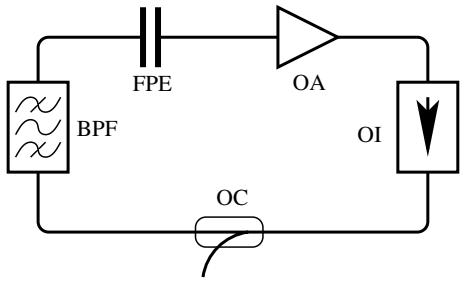

Figure 1. Fibre ring laser. OA-optical amplifier, OI-optical isolator, OC-output coupler, BPF-band-pass filter, FPE-Fabry–Perot etalon.

range (FSR) of the Fabry–Perot etalon. In the CGLE (1) we substitute the superposition of these three colinearly polarized monochromatic waves

$$u(z,t) = E_0(z,t) + E_s(z,t) + E_a(z,t) \tag{2}$$

where

$$E_0(z,t) = A_0(z)$$

$$E_a(z,t) = A_a(z)\exp\left\{\mathrm{i}\left[\frac{\beta_2\Omega^2}{2}z - \Omega t\right]\right\}$$

$$E_s(z,t) = A_s(z)\exp\left\{\mathrm{i}\left[\frac{\beta_2\Omega^2}{2}z + \Omega t\right]\right\}.$$

We obtain the coupled system of three ordinary differential equations for amplitudes and one for relative phase. Let the sideband amplitude change slowly so that the amplifier gain can track this slow change of loss caused by the redistribution of energy between the frequency components and filtering. Since the sidebands grow from noise, we can assume without a large error that their initial amplitudes are the same. Using the integrals of motion, these equations can be reduced to the following system of coupled equations:

$$\begin{aligned}\frac{\mathrm{d}\eta}{\mathrm{d}\xi} &= -2\eta(1-\eta)\sin\varphi + t(1-\eta)\eta \\ \frac{\mathrm{d}\varphi}{\mathrm{d}\xi} &= (\kappa-1) + 3\eta - 2(1-2\eta)\cos\varphi\end{aligned} \tag{3}$$

where the usual normalization [11] was used:

$$\begin{aligned} A_j &= |A_j|\mathrm{e}^{\mathrm{i}\varphi_j} \qquad j \in \{0,\ a,\ s\} \qquad \xi = RPz \\ P &= \sum_{j=0,a,s} |A_j|^2 \qquad \eta = |A_0|^2/P \\ \Delta k &= \beta_2\Omega^2 \qquad \kappa = \Delta k/(RP) \\ \varphi &= \Delta k z + \varphi_a + \varphi_s - 2\varphi_0 \\ t &= -\ln(T(\Omega)^2)/(RPL) \end{aligned} \tag{4}$$

where $T(\Omega)$ is the transmission coefficient of the bandpass filter for the detuning Ω and L is the length of the resonator. For the derivation of this system of equations for an ideal single-mode optical fibre ($t = 0$) see, for example, [11].

Our next objective will be to characterize the fixed points of the coupled system of equations (3). The derivatives on the left-hand sides of these equations vanish at the fixed point $[\eta_0, \varphi_0]$. Using the linear stability analysis, it can be shown that the stable fixed points of equations (3) are

$$[\eta_0, \varphi_0] = \begin{cases} \left[1, \arccos\left(-\frac{\kappa+2}{2}\right)\right] & \text{for } \kappa \in [-4; \kappa_1] \cup [\kappa_2; 3] \\ [\eta_0^{(2)}, \varphi_0^{(2)}] & \text{for } \kappa \in [\kappa_1; -1/2) \\ [\eta_0^{(2)}, \varphi_0^{(3)}] & \text{for } \kappa \in (-1/2, \kappa_2] \end{cases} \tag{5}$$

where

$$\kappa_{1,2} = -2 \mp \sqrt{4 - t^2} \tag{6}$$

and

$$\eta_0^{(2)} = \frac{5 + 3\kappa - 2t^2 + |1 + 2\kappa|\sqrt{4-t^2}}{7 - 4t^2} \tag{7}$$

$$\varphi_0^{(2,3)} = \arccos\left(-\frac{3\sqrt{4-t^2} \mp (8 - 2t^2)}{4\sqrt{4-t^2} \mp 6}\right) = \arcsin(t/2). \tag{8}$$

No fixed point exists for $\kappa < -4$, where $\mathrm{d}\varphi/\mathrm{d}\xi < 0$, i.e. the phase $\varphi(\xi)$ is a monotonically decreasing function. Analogously, no fixed point exists for $\kappa > 3$ and the phase $\varphi(\xi)$ is a monotonically increasing function in this region. The normalized pump η must be real-valued according to its definition (4). This sets a limit $t^2 < 4$ in (7), or equivalently $T\exp(RPL) > 1$. This inequality states that the loss caused by filtration must be lower than the maximum non-depleted MI gain achieved for $\eta \to 1$ and $\varphi = \pi/2$.

Figure 2(*a*) shows the normalized central component power η_0 and the relative phase ψ_0 in the fixed point of the dynamical system as functions of the normalized detuning κ. It can be seen that $\eta = 1$ for $\kappa < \kappa_1$. This means that all the power remains concentrated in the central component, no modulation instability develops and the laser remains in the CW regime. Above the threshold κ_1, the pump becomes depleted and the sideband amplitude increases due to the MI. Solving equation (6) for κ_1 with respect to P we get the threshold power for the onset of MI:

$$P_{th} = \frac{D^2 + 4\ln^2(T)}{-4DRL} \qquad D = \beta_2\Omega^2 L. \tag{9}$$

The sidebands reach their maximum amplitude in the point $\kappa = -1/2$, where an abrupt change of the phase occurs. The phase depends on the transmission coefficient of the filter and for weak filtration it is close to zero when $\kappa < -1/2$. Above this point it is close to π. If we further increase κ we observe a second threshold κ_2. No MI can be observed above this point. It also means that no MI can be observed for a normal dispersion resonator, where $\kappa > 0$.

Having the coordinates η_0 and ψ_0 of the fixed point of the dynamical system, we can reconstruct the pulse train in the time domain

$$\begin{aligned} e(t,z) &= E_1 + E_0 + E_2 \\ &= \sqrt{P}\mathrm{e}^{\mathrm{i}\varphi_0}\left\{\sqrt{\eta_0} + \sqrt{2-2\eta_0}\mathrm{e}^{\mathrm{i}\psi_0/2}\cos[\Omega(t-t_0)]\right\} \end{aligned}$$

where $t_0 = -(\varphi_1 - \varphi_2)/(2\Omega)$. This is illustrated by figure 3(*a*)–(*c*) for various normalized detunings κ. A clean pulse train is generated for $\kappa = -2$. For $\kappa = -0.6$ we get small satellites

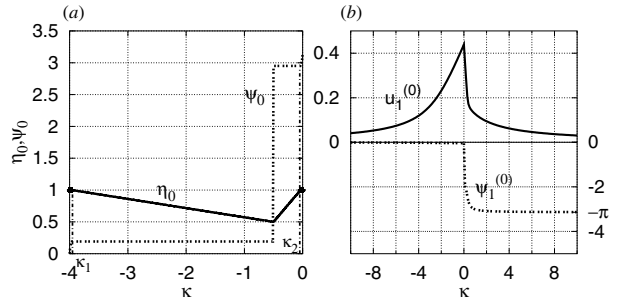

Figure 2. Dependence of stable fixed points coordinates on normalized detuning κ for three-wave model (a) and four-wave model (b).

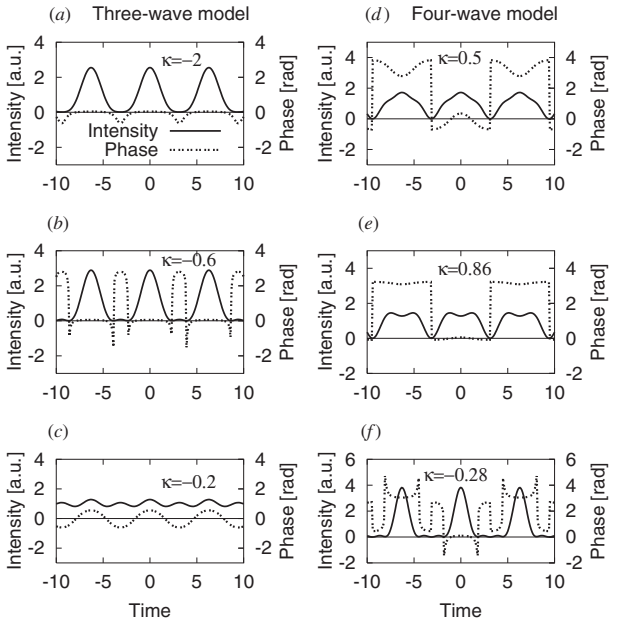

Figure 3. Pulse train reconstruction in time domain for three-wave model (a)–(c) and four-wave model (d)–(f).

between the pulses. The phase changes its sign whenever the intensity goes through zero. For $\kappa = -0.2$ small amplitude and pronounced phase modulations of the generated signal are obtained [12].

3. Four-wave model

If the bandpass filter is appropriately tuned in such a way that the filter transmission maximum falls in between two peaks of a Fabry–Perot etalon, a regime with an even spectrum is achieved. Let us suppose that in the steady state of the laser two lines (E_2, E_3) of the same amplitude initially exist. We will allow for the evolution of two sidebands (E_1, E_4) with the detuning Ω given by the FSR of the Fabry–Perot etalon. Substituting the superposition of these four waves

$$u(z,t) = E_1(z,t) + E_2(z,t) + E_3(z,t) + E_4(z,t)$$

where

$$\begin{aligned} E_{2,3}(z,t) &= A_{2,3}(z)\exp\left\{\mathrm{i}\left[\frac{\beta_2}{2}\left(\frac{\Omega}{2}\right)^2 z \pm \frac{\Omega}{2}t\right]\right\} \\ E_{1,4}(z,t) &= A_{1,4}(z)\exp\left\{\mathrm{i}\left[\frac{\beta_2}{2}\left(\frac{3\Omega}{2}\right)^2 z \pm \frac{3\Omega}{2}t\right]\right\} \end{aligned} \tag{10}$$

in the CGLE (1) and using a similar approach to that in the three-wave model, we can derive six coupled ordinary differential equations describing the evolution of four amplitudes and two relative phases, which can be reduced, using the assumption of initially equal sideband amplitudes and integrals of motion, to the system of two coupled equations:

$$\begin{aligned} \frac{\mathrm{d}u_1}{\mathrm{d}\xi} &= -(1-2u_1^2)\left\{\frac{1}{4}\sqrt{2-4u_1^2}\sin(\psi_1) + u_1[\sin(2\psi_1)-\delta]\right\} \\ \frac{\mathrm{d}\psi_1}{\mathrm{d}\xi} &= (1-4u_1^2)\left(\frac{1}{2} - 2\cos^2(\psi_1)\right) \\ &\quad + \frac{\cos(\psi_1)\sqrt{2-4u_1^2}}{4u_1}(8u_1^2-1) - \kappa \end{aligned} \tag{11}$$

where the following normalization was used:

$$\begin{gathered} A_j = |A_j|\mathrm{e}^{\mathrm{i}\varphi_j} \qquad j = \overline{1,4} \\ P_j = |A_j|^2 \qquad P = \sum_{j=1}^{4} P_j^2 \qquad u_j = |A_j|/\sqrt{P} \\ \psi_1 = 2\varphi_2 - \varphi_3 - \varphi_1 - \kappa z \\ \delta = t_1 - t_2 \qquad t_1 = -\ln(T(\tfrac{1}{2}\Omega)^2)/(RPL) \\ t_2 = -\ln(T(\tfrac{3}{2}\Omega)^2)/(RPL) \end{gathered} \tag{12}$$

and $T(\Omega)$ is the transmission coefficient of the bandpass filter for the detuning Ω. The linear stability analysis of this system was performed and stable fixed points were found numerically. An analytical expression for the fixed points in implicit form was found only for a special case of $\delta = 0$. The coordinates of the stable fixed points numerically obtained for $\delta = -0.36$ are shown in figure 2(b) as a function of the normalized detuning κ. We can see that the amplitude reaches its maximum value for $\kappa = 0$. Moreover, no threshold for the onset of MI was observed.

Having the coordinates $u_1^{(0)}$ and $\psi_1^{(0)}$ of the fixed point of the dynamical system, we can reconstruct the pulse train in the time domain:

$$\begin{aligned} e(t,z) &= E_1 + E_2 + E_3 + E_4 = 2\sqrt{P}\mathrm{e}^{\mathrm{i}\beta_2(\kappa z/8+\varphi)} \\ &\quad \times \left\{u_1^{(0)}\mathrm{e}^{-\mathrm{i}\psi_1^{(0)}}\cos\left[\frac{3\Omega(t-t_0)}{2}\right] + u_2^{(0)}\cos\left[\frac{\Omega(t-t_0)}{2}\right]\right\} \end{aligned} \tag{13}$$

where $t_0 = (\varphi_2 - \varphi_3)/\Omega$. Analysing the generated pulse train in the time domain, we can see that successive pulses have different phases. This is a characteristic feature of the even spectrum regime. The periodic solution may resemble a train of bright solitons with alternating phase (figure 3(f)) or a train of dark solitons (figure 3(e)).

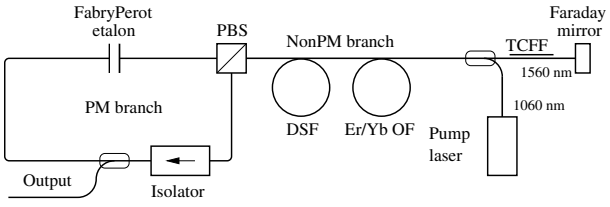

Figure 4. Experimental set-up of an MI σ-laser.

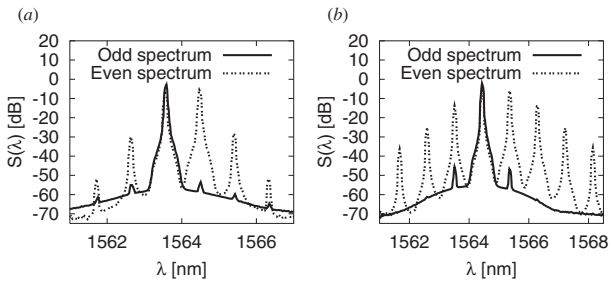

Figure 5. Spectrum for normalized detuning (a) below the first threshold κ_1 ($\kappa = -14.1$), (b) above the second threshold κ_2 ($\kappa = 0.5$).

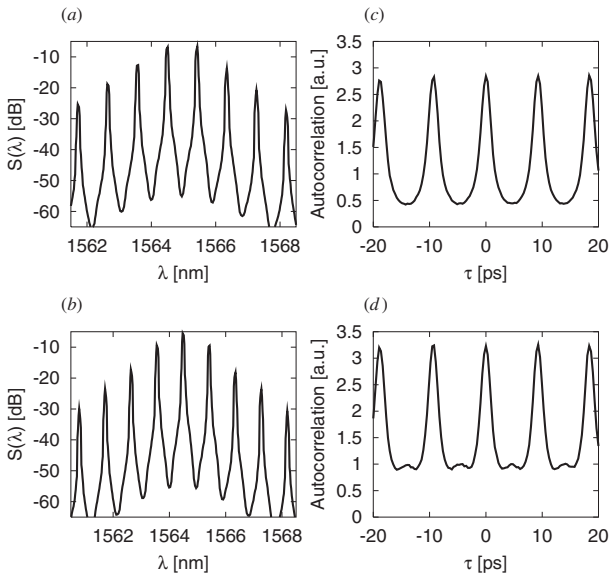

Figure 6. Spectra and autocorrelations for even spectrum regime (a), (b), and odd spectrum regime (c), (d).

4. Experimental results

The MI fibre σ-laser described in detail in [8] was used in experiments (figure 4). It acts essentially as a polarization maintaining (PM) unidirectional ring laser and its behaviour can be qualitatively described by the FRL models given in sections 2 and 3. The σ-configurations have been chosen with regard to the stability of the laser. The laser is composed of an unidirectional PM loop and a bidirectional non-PM branch connected together with a polarizing beamsplitter (PBS). The non-PM branch contains $\sim$10 m of an Er/Yb-doped optical fibre, pumped by an ytterbium fibre laser with an available output power of up to 5 W at 1060 nm. The pulses are formed in a section with a dispersion-shifted fibre (DSF) that actually represents combinations of non-zero dispersion fibres (NZDF) with dispersions of 1.6 ps^2 km^{-1} and -5.35 ps^2 km^{-1} and various lengths, allowing us to set an appropriate average dispersion of the resonator. An average nonlinear coefficient of fibres was taken to be $R = 1.35$ W^{-1} km^{-1} at a wavelength of 1560 nm. The spectral filtration is achieved in a two-core fibre filter with a FWHM bandwidth of 4.2 nm [8]. The birefringence variations of the non-PM branch are compensated for by a Faraday mirror. At the same time the Faraday mirror prevents spatial hole burning from occurring in the active fibre. The PM loop contains only an isolator, a 70% output coupler and the Fabry–Perot etalon with a free spectral range of 107.2 GHz and a finesse of 300 that defines the repetition rate of the laser. The suppression of MI for normalized detuning below the first threshold κ_1 (an average dispersion of the resonator was $\bar{\beta}_2 = -21.64$ ps^2 km^{-1}, corresponding to a normalized detuning of $\kappa = -14.1$ for an intracavity signal power of 0.516 W and an effective length was 233.5 m) and above the second threshold κ_2 ($\bar{\beta}_2 = 0.86$ ps^2 km^{-1} corresponding to $\kappa = 0.5$ for an intracavity signal power of 0.578 W and an effective length was 225.5 m) is documented in figure 5. Here the sidebands are strongly suppressed in the odd-spectrum regime. For the same normalized detunings κ, the sidebands are well developed in the even-spectrum regime. The ratio of amplitudes of the nearest sidebands to the main peaks for a normalized detuning of $\kappa = 0.5$ is higher than for $\kappa = -14.3$ by an amount of 15 dB, consistent with the four-wave model that predicts a difference of 18 dB. In an anomalous dispersion resonator and for appropriate normalized detunings both the even- and odd-spectrum regimes may exist, as can be seen in figure 6(a), (b). For this configuration an average dispersion of the resonator was $\bar{\beta}_2 = -0.5$ ps^2 km^{-1} and the effective length of the resonator was 345.5 m. The MI regime sets for the signal power of 150$\pm$7 mW. This is in excellent agreement with an estimated signal threshold power of 145 mW according to equation (9). Consistent with the three-wave model, the threshold power decreased to 100 mW when a Fabry–Perot etalon with a FSR of 107 GHz was replaced by one with a FSR of 88.5 GHz. Figure 6(c), (d) shows autocorrelations that correspond to spectra in figure 6(a), (b). An apparent background in the autocorrelation is caused by autocorrelating pulses with a large duty cycle. This can be directly seen for the even-spectrum regime where the intensity should go through zero between the successive pulses. Qualitatively similar autocorrelations can be obtained from pulse trains shown in figure 3. However, direct comparison with predicted autocorrelations cannot be done since real pulses are shorter than pulses obtained from simple truncated models due to higher harmonic contents.

5. Conclusions

The three- and four-wave models of an MI-based fibre ring laser were derived. Steady-state regimes of the MI FRL were found and their asymptotic stability was analysed by linear stability analysis. The three-wave model gives simple analytical expressions, allowing us to estimate the MI regime threshold power. The four-wave model predicts no threshold for the onset of MI and allows for the induced MI regime in FRL with a normal dispersion resonator. These features have been verified experimentally using the MI fibre σ-laser.

Acknowledgment

This work was done under grants nos 102/98/P235 and 102/99/0393 of the Grant Agency of the Czech Republic.

References

[1] Hasegawa A and Brinkman W F 1980 *IEEE J. Quantum Electron.* **16** 894
[2] Tai K, Hasegawa A and Tomita A 1986 *Phys. Rev. Lett.* **56** 135
[3] Trillo S and Wabnitz S 1989 *J. Opt. Soc. Am.* B **6** 238
[4] Hasegawa A 1984 *Opt. Lett.* **9** 288
[5] Tai K, Tomita A, Jewell J L and Hasegawa A 1986 *Appl. Phys. Lett.* **49** 236
[6] Franco P *et al* 1995 *Opt. Lett.* **20** 2009
[7] Yoshida E and Nakazawa M 1997 *Opt. Lett.* **22** 1409
[8] Honzatko P, Peterka P and Kanka J 2001 *Opt. Lett.* **26** 810
[9] Haus H A 2000 *IEEE J. Selected Topics Quantum Electron.* **6** 1173
[10] Porubov A V and Velarde M G 1999 *J. Math. Phys.* **40** 884
[11] Cappellini G and Trillo S 1991 *J. Opt. Soc. Am.* B **8** 824
[12] Trillo S and Wabnitz S 1991 *Opt. Lett.* **16** 1566
[13] Haelterman M, Trillo S and Wabnitz S 1994 *Opt. Lett.* **11** 446
[14] Coen S and Haelterman M 1998 *Opt. Commun.* **146** 339